A FREQUENCY DOMAIN SYSTEM MODEL WITH COUPLED MODES FOR LIMIT CYCLE PREDICTION OF THERMOACOUSTIC SYSTEMS

Fatih Selimefendigil, Wolfgang Polifke*

Lehrstuhl für Thermodynamik, TU München
Boltzmannstr. 15, D-85748, Germany
*Corresponding author: polifke@td.mw.tum.de

To predict the limit cycle oscillations of thermo-acoustic systems, a frequency-domain, low-order system model with explicit modal coupling is developed. To this purpose, a model for the nonlinear heat source dynamics is obtained from unsteady computational fluid dynamics in combination with feed-forward neural network identification. From the neural network, an equivalent representation for the input-output relation in Volterra series form is derived, where Volterra kernels are computed in terms of the weights of the neural network. Then the kernels are transformed into the frequency domain to obtain the higher order transfer functions, through which the modes are coupled. In this way nonlinear energy exchange among the modes can be described explicitly. Comparison with a Galerkin time domain simulation shows that deviations from purely sinusoidal behaviour in the limit cycle are captured correctly, while the computational cost is drastically reduced.

1 Introduction

In thermoacoustic systems, nonlinear effects limit the growth of unstable modes of oscillation and lead to steady state, periodic, nonlinear oscillations, which are called "limit cycle". As it is not always possible to avoid thermo-acoustic instabilities altogether, it is important to predict and analyze the oscillations in the limit cycle, since the detrimental effects of instabilities on combustor lifetime and noise emissions depend on the limit cycle amplitude.

Accurate predictions of the stability limits and limit cycle amplitudes require an adequate heat source model valid in the nonlinear regime as well as a suitable system model. CFD computations of the full thermo-acoustic system could model the limit cycle. These computations generally demand huge computational resources and time, since thermo-acoustic instabilities involve various physical phenomena covering a wide range of length and time scales [28, 36], and they depend in an sensitive manner on combustor operating conditions. For practical design purposes, a full CFD modeling approach for thermo-acoustic limit cycles is not feasible.

However, if the heat source is the dominant nonlinear element in the system – which is often the case – then it is possible to combine a linear model for the acoustics with a nonlinear model for the heat source. For example, from linearized thermo-fluid-dynamics equations the inhomogeneous wave equation for pressure fluctuations with a source term, which represents the heat release rate from combustion [22,25], can be derived and solved with a Finite Element or Finite Volume method. Approximate solutions of the inhomogeneous wave equation can also be obtained with the Galerkin method [5,6,39]. In the Galerkin method, acoustic velocity and pressure are expressed in terms of basis functions, which satisfy the boundary conditions and constitute a complete set of basis. The computations will often be cheaper than the former approach. Both the inhomogeneous wave equation and the Galerkin method

can predict the limit cycle amplitudes, if combined with a nonlinear model for the heat source. However, if the dynamic model of the heat source has many delay terms, a delay differential equation (DDE) results in the Galerkin time domain equations. Numerical integration of this delay differential system is computationally expensive.

Frequency domain system models are an attractive alternative, since they require to solve only a comparatively small set of algebraic equations instead of partial differential equations. Linear frequency domain "network models" of thermo-acoustic system have been developed by several researchers, see e.g. [7, 9, 10, 18]. In this approach, individual elements of thermo-acoustic network are described by their transfer functions/matrices which could be derived analytically, measured from the experiments or computed from the numerical simulations. Polifke and co-workers have used linear system identification method as an effective tool to construct transfer functions/matrices using input-output data set generated from unsteady CFD computations [15, 16, 29, 35].

Linear network models can predict the frequency and the growth rate of unstable modes, but are incapable of predicting limit cycle amplitudes. Fortunately, the models can be extended to the nonlinear regime with the "describing function" method [8, 23]. The (sinusoidal) describing function of a nonlinear element is an amplitude dependent frequency response sinusoid input [8, 14, 23]. In thermoacoustic systems, the heat source is often considered to be the dominant nonlinear element. If a sinusoidal input is applied, the nonlinear heat source produces higher harmonics at multiple integers of the fundamental harmonic. When the system acoustic filters these higher harmonics, or if the flame response is very weak at the corresponding frequencies, a one-mode approximation for the limit cycle behaviour is obtained. Moreover, sub-critical bifurcations can be predicted with this method [23].

The describing function approach neglects the effect of coupling terms, since it is a one mode (sinusoid) approximation. The aim of the present study is to develop a frequency domain system model with explicit modal coupling. Acoustic velocity and pressure fluctuations at large amplitudes are thus expressed as a superposition of several modes. The nonlinearity in the heat source is expressed in terms of higher order transfer functions through which the modes are coupled. A schematic representation of the approach is shown in Fig. 1: from a CFD model for the heat source dynamics, higher order transfer functions are determined via an extension of the neural network identification method to the frequency domain. Combined with a frequency domain model for the system acoustics with modal coupling, limit cycle amplitudes can be predicted. Note that Fig. 1 indicates also how the CFD time series data can be used to identify a nonlinear heat source model for a time domain Galerkin model in terms of a neural network. This alternative is used in the present paper for cross-validation purposes.

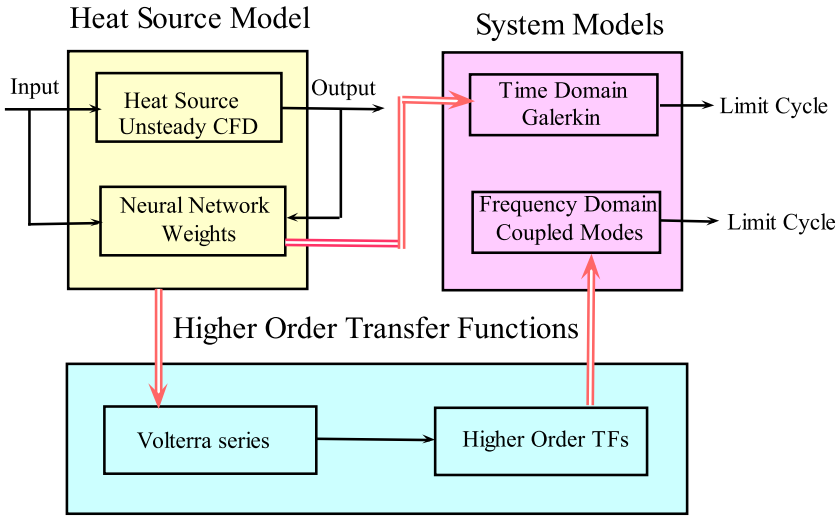

Figure 1: Schematic of the proposed approach from the nonlinear identification of the heat source to the simulation in time and frequency domain for the full thermo-acoustic system

The paper is organized as follows: firstly, the CFD model of the heat source is reviewed briefly, details can be found in [7, 29]. Secondly, system identification based on neural networks is discussed. Volterra kernel extraction and the extension to the frequency domain to obtain the higher order transfer functions are illustrated. Then the Galerkin time domain method for one dimensional acoustics is introduced, since the limit cycle can be predicted with this method and our system model equations for the frequency domain with the coupled modes have been derived from this method. Finally, the frequency domain system model with coupled modes is described. When the input to the heat source is expressed as superposition of the modes, then these will be coupled through the higher order transfer functions (when the heat source nonlinearity is expressed in terms of higher order transfer functions). Simulation results obtained with the Galerkin time domain method, the describing function method and the coupled modes system model, respectively, are compared against each other. It is found that the frequency domain model is computationally efficient compared to a time domain simulation and it does – unlike the describing function model – capture correctly the non-sinusoidal shape of limit cycle oscillations. Moreover, the energy exchange between the modes (from the fundamental to higher order modes and *vice versa*) can be analyzed with this model. To conclude the analysis of results, the Rayleigh index in the nonlinear regime and in particular the contributions of the individual modes to the Rayleigh index are evaluated.

2 Numerical Simulation of the Heat Source in Pulsating Flow with Unsteady CFD

A simple thermoacoustic device is the Rijke tube (Fig. 2), in which a hot wire gauze is located inside a tube. A mean flow of gas is induced by free or forced convection, and heat is transferred from the gauze to the gas. A CFD model representing one wire of the mesh as a cylinder in cross flow has been constructed, see Fig. 3.

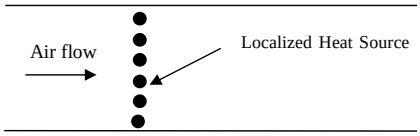

Figure 2: Schematic of the Rijke tube with a concentrated heat source

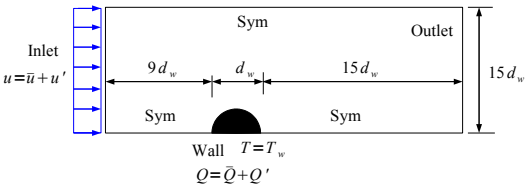

Figure 3: Geometry and boundary conditions for CFD modeling of a single wire

Karman vortex streets downstream of a cylinder are observed at Re > 40. In the present case, the Reynolds number Re = 15, such that Karman vortices are absent. The use of symmetry boundary conditions at the top and bottom of the domain to reduce the size of the computational domain is thus justified. The body-fitted mesh is composed of 16540 quadrilateral elements and is refined close to the cylinder surface. Mesh independence of the solutions has been confirmed. The unsteady Navier-Stokes equation along with the energy equation is solved using FLUENT 6.1 segregated solver (a general purpose finite volume solver) [12]. In the CFD model, an appropriate perturbation signal (a chirp signal of varying amplitude) for the nonlinear system identification is imposed on the steady state solution, which is used as the initial condition for the unsteady calculation. The heat transfer rate is extracted as the area-integral averaged values over the wire. More details about the model can be found in [13, 32].

3 Neural Network Identification

For highly nonlinear systems, *black box identification* can be used if little or no priori information about the complex physics is available [17, 34]. *Neural network identification* methods belong to the class of

parametric nonlinear black box identification procedures [21, 24, 27, 34]. They are promising to identify any nonlinearity up to a specified degree of accuracy (universal function approximators).

For the present case of a wire in pulsating cross flow, nonlinear complex interactions take place in the boundary layer once the pulsating flow velocity achieves high values. It is possible to obtain a dynamic model (input-output relation) that is valid for a range of amplitudes and frequencies with nonlinear black box identification from measured input and output time series data [32, 33]. Nonlinear dynamic models of more advanced configurations of the heat source (e.g. turbulent combustion) can in principle also be obtained with this approach. Fig. 4 shows the neural network identification scheme for the nonlinear heat source.

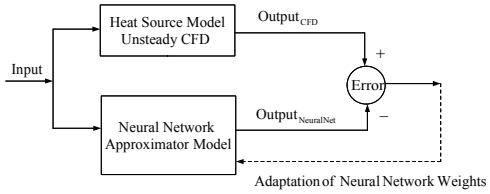

Figure 4: Nonlinear identification using unsteady CFD and Neural Network approximation

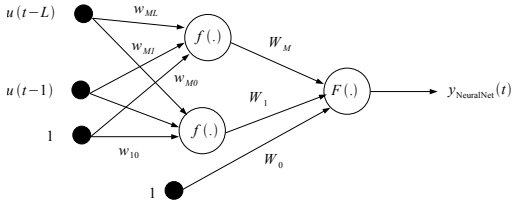

Figure 5: 1 hidden layer feed-forward neural network structure along with regressors with tangent hyperbolic activation function f and the linear function F at the output layer, M is the number of units and L is the memory length of the regressors

Network structures can be classified as feed-forward or recurrent [21, 27]. In a recurrent network structure, the computed outputs from the network will be fed as the input to the layers. In this study we use a feed-forward network structure and we only consider past inputs as the input to the neural network (NFIR model). The network has only 1 hidden layer and tangent hyperbolic as the activation function. A schematic of the neural network topology along with the regressors used as the input is shown in Fig. 5. Let φ be the set of regressors with memory length of L, u as the input, y as the output

$$\phi = [1\ u(t-1)\ ....u(t-L)], \tag{1}$$

and Z^N be the set of the input-output data (training set) up to time N. Then the identification problem will be formulated as the minimization of the error between the CFD model output and the output from neural network as

$$V_N(\theta) = \frac{1}{N}\sum_{t=1}^{N}[y_{\mathrm{CFD}}(t) - y_{\mathrm{NeuralNet}}(t)]^2. \tag{2}$$

This function will be minimized by some nonlinear iterative search algorithms and we use Levenberg-Marquardt technique to find the minimum of the function and hence the weights of neural networks which are denoted by θ . The output from the neural network will be written in terms of the weights of the network as

$$y_{\mathrm{NeuralNet}}(t) = \sum_{j=1}^{M} W_j f(\sum_{l=1}^{L} w_{jl}\phi_l + w_{j0}) + W_0, \tag{3}$$

where w and $W's$ are the weights of the neural network for the input and output to the hidden layer and f is the tangent hyperbolic activation function.

3.1 Extraction of Kernels in terms of Neural Network Weights

As mentioned before, a wide class of nonlinear systems can be represented in Volterra series form for the input-output relation (extension of the Taylor series approximation for functionals [3, 4]). For an

input-output data set $(u(t), y(t))$ with memory length L, this relation will be written for a third order nonlinearity in discrete form as

$$y(t) = h_0 + \sum_{\tau=1}^{L} h_1(\tau)u(t-\tau) + \sum_{\tau_1=1}^{L}\sum_{\tau_2=1}^{L} h_2(\tau_1,\tau_2)u(t-\tau_1)u(t-\tau_2) + \sum_{\tau_1=1}^{L}\sum_{\tau_2=1}^{L}\sum_{\tau_3=1}^{L} h_3(\tau_1,\tau_2,\tau_3)u(t-\tau_1)u(t-\tau_2)u(t-\tau_3). \quad (4)$$

Different approaches exist in the literature to extract the kernels. A correlation based analysis with broadband forcing has been developed by Schetzen et al. [31]. This method requires lengthy signals and the number of the parameters (h coefficients) is huge. A orthogonalization of the above expression using a Gram-Schmid algorithm has been purposed by Korenberg et al. [19]. This has the advantage not to require a specific type of (like broadband) signal for the excitation of the system. Wray et al. [37] have developed a strategy to get an improved accuracy of the nonlinear approximation in comparison to Toeplitz matrix inversion proposed by Korenberg et al. [19]. In this study, we use the approach proposed by Wray et al. [37]. The idea is to expand the neural network approximation output as in Eq. (3) for the tangent hyperbolic function around the bias term. Taylor series approximation of the tangent hyperbolic function around zero can be written as [37]

$$\tanh(x) = \sum_{n=1}^{\infty} (-1)^{n+1} \frac{B_n(2^{4n}-2^{2n})x^{2n-1}}{(2n)!}, \quad (5)$$

where B_n is the n th order Bernoulli number and is defined as

$$B_n = \frac{2(2n)!}{(2\pi)^{2n}} \sum_{s=1}^{\infty} \frac{1}{s^{2n}}. \quad (6)$$

Expanding the activation function in Eq. (3), the neural network output will be written as

$$y_{\mathrm{NeuralNet}}(t) = \sum_{j=1}^{M} W_j \left[\frac{\sum_{k=1}^{\infty} (-1)^{k+1} B_k(2^{4k}-2^{2k}) \left(\sum_{l=1}^{L} w_{jl}\phi_l + w_{j0} \right)^{2k-1}}{(2k)!} \right] + W_0. \quad (7)$$

Combining this representation with Volterra series of third order in the form as in Eq. (4), we will express the kernels in terms of the weights of the neural network.

The zeroth order kernel:

$$h_0 = \sum_{j=1}^{M} W_j \left[\frac{\sum_{k=1}^{\infty} (-1)^{k+1} B_k(2^{4k}-2^{2k}) C(2k-1,0) w_{j0}^{2k-1}}{(2k)!} \right] + W_0. \quad (8)$$

The first order kernels:

$$h_1(a) = \sum_{j=1}^{M} W_j \left[\frac{\sum_{k=1}^{\infty} (-1)^{k+1} B_k(2^{4k}-2^{2k}) C(2k-1,1) w_{ja} w_{j0}^{2k-2}}{(2k)!} \right], a = 1, \ldots, L. \quad (9)$$

and the definition of the nth order kernel can be given as

$$h_n(a_1,..,a_n) = \sum_{j=1}^{M} W_j \left[\frac{\sum_{k=1}^{\infty} (-1)^{k+1} B_k \left(2^{4k}-2^{2k}\right) C(2k-1,n)\, w_{ja_1}..w_{ja_n} {w_{j0}}^{2k-n-1}}{(2k)!} \right], \quad (10)$$

$$\text{with } a_i = 1,\ldots,L \text{ for } i = 1,\ldots,L, \text{ while } C \text{ is defined as}$$

$$C(m,n) = \begin{cases} \frac{m!}{n!(m-n)!} & \text{for} \quad m \geq n \\ 0, & \text{otherwise.} \end{cases} \quad (11)$$

3.2 Higher Order Transfer Functions

Once the kernels of various orders are calculated, these will then be extended into frequency domain to obtain the higher order transfer functions. When the system experiences different frequencies, one can see how the nonlinearity of the system effects these frequencies in order to produce sum of the frequencies, differences between the frequencies which are typical for a nonlinear system. For a thermoacoustic system, these transfer functions allow us to see how different modes interact with each other and transfer energy to higher order modes. The first order transfer function will be computed from z-transform of the first order kernel as,

$$H_1(\omega) = \sum_{k=1}^{L} h_1(k) e^{-i\omega k\Delta t}. \quad (12)$$

The third order transfer function will be computed from z-transform along the three frequency directions of the third order kernel and will be written as

$$H_3(\omega_1,\omega_2,\omega_3) = \sum_{k=1}^{L}\sum_{l=1}^{L}\sum_{m=1}^{L} h_3(k,l,m) e^{-i\omega k\Delta t} e^{-i\omega l\Delta t} e^{-i\omega m\Delta t}. \quad (13)$$

Suppose that the system experiences a sinusoid input with amplitude U_0 and frequency ω,

$$u(t) = U_0 \sin(\omega t) = U_0 \left(\frac{e^{i\omega t} - e^{-i\omega t}}{2i} \right). \quad (14)$$

Then the corresponding output in the frequency domain in terms of the higher order transfer functions will be computed as

$$Y(\omega) = U_0 H_1(\omega) + \frac{3{U_0}^3}{4} H_3(\omega,\omega,-\omega). \quad (15)$$

In this expression, the contribution of the nonlinearity is seen in the third order transfer function. The advantage of this representation of the nonlinearity will be clearer when a frequency domain thermoacoustic system model is developed.

3.3 Nonlinear Identification of the Wire in Pulsating Flow from CFD and Neural Network based Identification

As the input to the heat source, a chirp signal of varying amplitudes is used with Str ranges from 0.72 to 2.88. The perturbation amplitudes are A = 0.3, 1, 1.5 and 2. Non-dimensional amplitude and the frequency of the forcing; velocity amplitude ratio (A) and Strouhal Number (Str) are defined as

$$\mathrm{A} = \frac{u'}{\bar{u}}, \quad (16)$$

$$\mathrm{Str} = \omega \frac{d_w}{\bar{u}}, \quad (17)$$

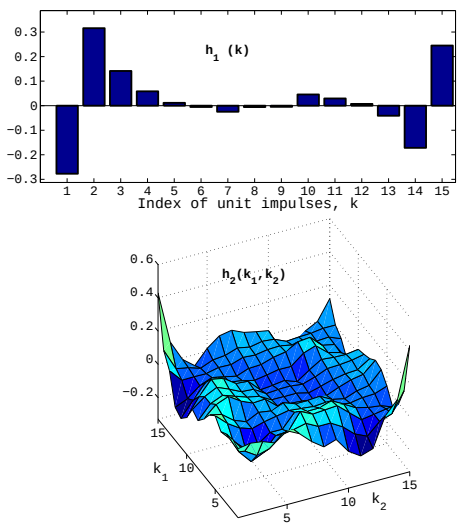

Figure 6: First (top) and second (bottom) order kernels (Number of the regressors is 15)

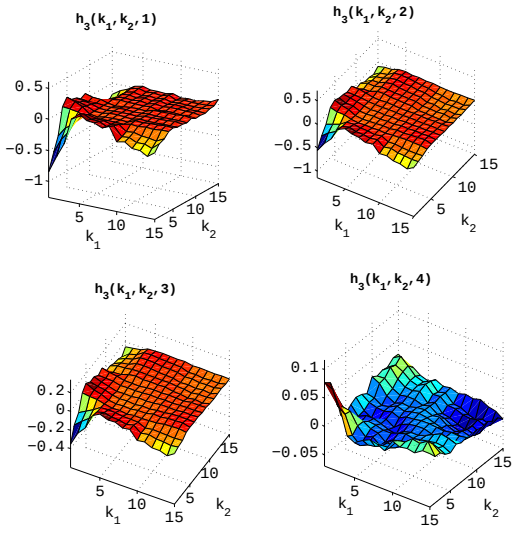

Figure 7: Third order kernels for values $k_3 = 1,\ldots,4$ for the third dimension

for fluctuating velocity u', forcing radial frequency ω, wire diameter d_w and the mean velocity $\bar{u}$. The chirp signal has linearly varying frequency component over time and is defined for one amplitude of the forcing

$$u(t) = \bar{u} + \mathrm{A}\bar{u}\sin\left(\left(\omega_{\max} - \left(\frac{\omega_{\max} - \omega_{\min}}{M}k\right)\right)k\Delta t\right), \quad k = 1,2,\ldots,M, \tag{18}$$

with maximum and minimum frequencies of $\omega_{\min}$, $\omega_{\max}$ and amplitude A. M, Δt denote the number of the total samples used and time step, respectively. The memory length of the regressors is 15 and the neural network is a structure with one hidden layer and 12 neurons, composed of tangent hyperbolic functions and a linear output layer. The fits for the nonlinear approximations with the neural network along with Volterra series approximation up to third order, to the CFD output is 86%. Next the kernels of various orders are extracted with the procedure outlined in the previous section. Fig. 6 shows the first and second order kernels. The value of the h_0 is -0.00186. For a sinusoidal input, the output from the heat source model will be calculated using Eq. (15) in terms of higher order transfer functions and amplitude of the sinusoid. A comparison with the single sinusoidal response from CFD is shown for $\mathrm{A} = 1.5, 2$ and for $\mathrm{Str} = 1.08, 1.8, 2.16, 2.88$ in Fig. 8 along with a linear transfer function. The maximum deviation is observed at $\mathrm{A} = 1.5$ and $\mathrm{Str} = 1.08$, but this is less than 6%, and overall agreement between the model output and CFD output is adequate for the considered range of amplitudes and the frequencies.

4 Time Domain Simulation

4.1 Galerkin Method

In this modeling approach, acoustic velocity and pressure are expressed in terms of a set of basis functions, which constitute a complete basis and satisfy the boundary conditions [1, 5, 6]. Using the orthogonality of the basis functions, partial differential equations are projected onto the basis functions and one has to solve a set of ordinary differential equations instead of partial differential equations. Even though, the method used here is for a simple geometry (Rijke tube), it can be applied to complex geometries of practical interest, as well. In this case (complex geometry case, including also more general boundary conditions), the basis functions (mode shapes) could be obtained from a three dimensional finite element simulation of the acoustics of the system [2]. Acoustic variables (pressure and velocity)

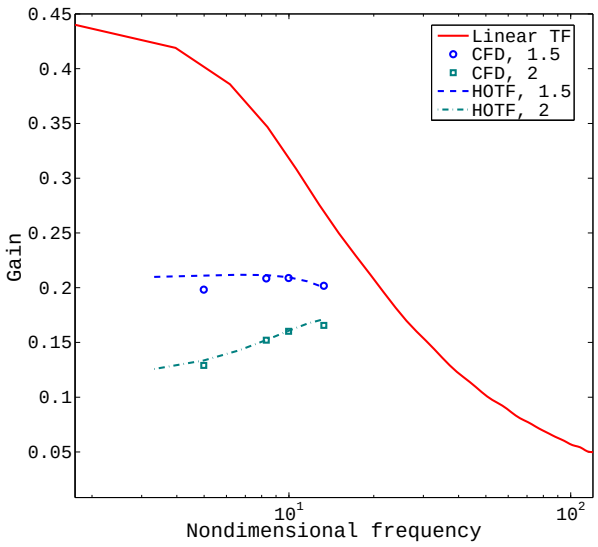

Figure 8: Gain of the transfer function calculated from CFD for single sinusoidal input (A = 1.5,2, Str = 1.08,1.8,2.16,2.88), and obtained from higher order transfer functions along with a linear transfer function on a semi-logarithmic plot

are then written as the superposition of these mode shapes with the time dependent coefficients. In the Galerkin method, acoustic velocity and pressure will be written in terms of the natural modes of the duct [5,6],

$$u'(x,t) = \sum_{m=1}^{N} \eta_m(t)\cos(m\pi x), \quad p'(x,t) = -\sum_{m=1}^{N} \frac{\gamma \mathrm{Ma}}{m\pi}\dot{\eta}_m(t)\sin(m\pi x). \tag{19}$$

Using the above expansions for the acoustic velocity and pressure in the governing equations and integration over the domain will result in a set of ordinary differential equations for the time dependent coefficients of the expansion as,

$$\frac{d^2\eta_j}{dt^2} + 2\xi_j\omega_j\frac{d\eta_j}{dt} + {\omega_j}^2\eta_j = \frac{2(1-\gamma)}{\mathrm{Ma}\,c_0 p_0 \gamma} j\pi \sin(j\pi x_f)Q', \tag{20}$$

with $\omega_j = j\pi$. The damping coefficients have been determined by Matveev experimentally and given with the following relation [20]

$$\xi_j = \frac{1}{2\pi}\left(c_1\frac{\omega_j}{\omega_1} + c_2\sqrt{\frac{\omega_1}{\omega_j}}\right). \tag{21}$$

A detailed derivation of the equations can be found in [1,9]. In the above equations, the heat source is written explicitly and in the case of a heat source model from linear/nonlinear system identification, one has to solve a delay differential equation with multiple fixed delays. If the number of the fixed delays is large, the computations may be time consuming.

4.2 Simulation with the CFD/SI Model of the Wire Heat Source

The dynamic model of the heat source (wire in pulsating flow) obtained from a neural network identification procedure has been used in time domain Galerkin simulation. Matlab DDE solver is used to solve the delay differential equations with the delays resulting from the identification part. For the first configuration, the heat source is located at $0.15L$ downstream of the tube inlet with the tube length L. Total time of the simulation is set to 1000 non-dimensional time and a five mode approximation is utilized. In the second configuration, the heat source location is set to $0.25L$ downstream of the tube inlet

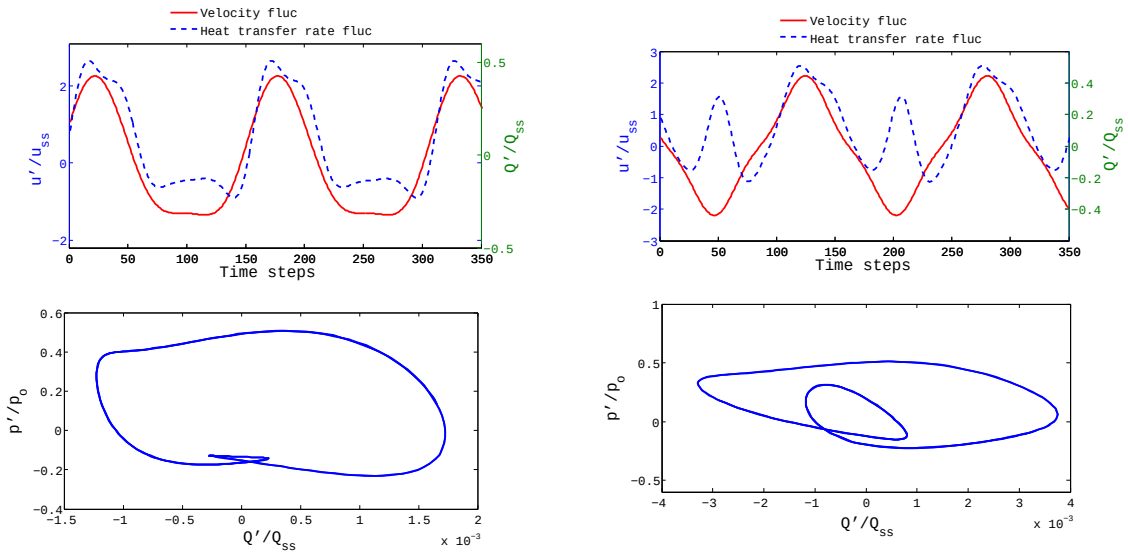

Figure 9: Limit cycle behaviour for duct length $L = 5.65$, damping coefficients c_1 =0.0135, c_2 =0.0015. Top: Non-dimensional acoustic velocity and heat transfer rate vs. time. Bottom: Phase portrait of the acoustic pressure versus heat transfer rate. Left: Initial conditions $\eta_1(0) = 0.02$, heat source at $x_f = 0.15L$. Right: $\eta_1(0) = 0.02$, heat source at $x_f = 0.25L$.

and the simulation time is 1500 (non-dimensional time).

Fig. 9 shows the normalized heat transfer rate (with respect to the steady state value) and acoustic quantities u' and p' in the limit cycle as time series and phase portraits, respectively. Two cases are considered: heat source located at $x_f = 0.15L$ (left) and $x_f = 0.25L$ (right). These plots indicate how the heat source acts as a nonlinear element. The computational time for these simulations varies between 10-13 hours on a 64-Bit processor with 2.8 GHz.

5 Frequency Domain System Model with Coupled Modes

In this system modeling approach, it is assumed that the main source of the nonlinearity is due to the heat source for a thermo-acoustic system. A model of the heat source has been obtained from neural network based nonlinear identification using input-output data set generated from the unsteady CFD computations. A polynomial representation of the input-output is obtained after an approximation of the expansion function (tangent hyperbolic) used in the units of the neural network with polynomials. Extensions of the linear transfer function to higher dimensions, the so-called higher order transfer functions are obtained in the frequency domain. Details of the procedure to compute the higher order transfer functions have been described before in the previous chapter. This type of representation of the nonlinearity has great advantages when used in a modal basis representation of the thermo-acoustic system. It allows the input to the the heat source to be sum of the modes and accounts for the interaction of the modes. An analysis of the energy balance (harmonic balance) of the modes (transfer of energy from the fundamental mode to the higher order modes and contribution of the higher order modes to the fundamental mode) is possible with this approach. Rayleigh index in the nonlinear regime can be studied and the contribution of the higher order modes to this index can be found out. In the current version, Galerkin time domain equations are used in which the system variables (acoustic velocity and pressure) are expressed as sum of the modes, but linear network modeling approach can also be used as well for an extension into the nonlinear regime with this nonlinear representation of the heat source.

5.1 Derivation

The evolution coefficient in front of the mth mode in the frequency domain can be written as

$$\eta_m(t) = A_m \sin(\omega_m t) + B_m \cos(\omega_m t) = \left(\frac{B_m}{2} + \frac{A_m}{2i}\right) e^{i\omega_m t} + \left(\frac{B_m}{2} - \frac{A_m}{2i}\right) e^{-i\omega_m t}. \tag{22}$$

Let us denote the

$$C_m = \frac{B_m}{2} + \frac{A_m}{2i}, \quad D_m = \frac{B_m}{2} - \frac{A_m}{2i}. \tag{23}$$

Then the time derivatives become

$$\frac{d\eta_m(t)}{dt} = i\omega m C_m e^{i\omega m t} - i\omega m D_m e^{-i\omega m t}, \tag{24}$$

$$\frac{d^2\eta_m(t)}{dt^2} = -(\omega m)^2 C_m e^{i\omega m t} - (\omega m)^2 D_m e^{-i\omega m t}. \tag{25}$$

Next, the heat source model will be obtained in terms of coupled modes. The input to the heat source (acoustic velocity in the immediate vicinity) is assumed to be sum of the modes

$$u'(t) = \sum_{m=1}^{N} \eta_m(t) \cos(m\pi x) = \sum_{m=1}^{N} \left(C_m e^{i\omega m t} + D_m e^{-i\omega m t}\right) \cos(m\pi x_f). \tag{26}$$

On substituting this for the input in the polynomial input-output representation and using the definitions of the higher order transfer functions, the corresponding output will be obtained in terms of the couped modes as

$$\begin{aligned}
Q'(t) = & \sum_{d_1=1}^{N} \left(C_{d_1} H_1(\omega d_1)\, e^{i\omega d_1 t} + D_{d_1} H_1(-\omega d_1)\, e^{-i\omega d_1 t}\right) \cos(\pi d_1 x_f) \\
& + \sum_{d_1=1}^{N} \sum_{d_2=1}^{N} \begin{pmatrix} C_{d_1} C_{d_2} H_2(\omega d_1, \omega d_2)\, e^{i\omega(d_1+d_2)t} \\ +C_{d_1} D_{d_2} H_2(\omega d_1, -\omega d_2)\, e^{i\omega(d_1-d_2)t} \\ +D_{d_1} C_{d_2} H_2(-\omega d_1, \omega d_2)\, e^{i\omega(-d_1+d_2)t} \\ +D_{d_1} D_{d_2} H_2(-\omega d_1, -\omega d_2)\, e^{i\omega(-d_1-d_2)t} \end{pmatrix} \cos(\pi d_1 x_f) \cos(\pi d_2 x_f) \\
& + \sum_{d_1=1}^{N} \sum_{d_2=1}^{N} \sum_{d_3=1}^{N} \begin{pmatrix} C_{d_1} C_{d_2} C_{d_3} H_3(\omega d_1, \omega d_2, \omega d_3)\, e^{i\omega(d_1+d_2+d_3)t} \\ +C_{d_1} C_{d_2} D_{d_3} H_3(\omega d_1, \omega d_2, -\omega d_3)\, e^{i\omega(d_1+d_2-d_3)t} \\ +D_{d_1} C_{d_2} D_{d_3} H_3(-\omega d_1, \omega d_2, -\omega d_3)\, e^{i\omega(-d_1+d_2-d_3)t} \\ +D_{d_1} D_{d_2} C_{d_3} H_3(-\omega d_1, -\omega d_2, \omega d_3)\, e^{i\omega(-d_1-d_2+d_3)t} \\ +C_{d_1} D_{d_2} C_{d_3} H_3(\omega d_1, -\omega d_2, \omega d_3)\, e^{i\omega(d_1-d_2+d_3)t} \\ +D_{d_1} C_{d_2} C_{d_3} H_3(-\omega d_1, \omega d_2, \omega d_3)\, e^{i\omega(-d_1+d_2+d_3)t} \\ +C_{d_1} D_{d_2} D_{d_3} H_3(\omega d_1, -\omega d_2, -\omega d_3)\, e^{i\omega(d_1-d_2-d_3)t} \\ +D_{d_1} D_{d_2} D_{d_3} H_3(-\omega d_1, -\omega d_2, -\omega d_3)\, e^{i\omega(-d_1-d_2-d_3)t} \end{pmatrix} \prod_{i=1}^{3} \cos(\pi d_i x_f).
\end{aligned} \tag{27}$$

In this representation, the modes are coupled through the higher order transfer functions. After substitution the time derivatives and heat source in terms of the higher order transfer functions in Eq. (20) and harmonic balancing (equating the exponentials of the same order), the equation for mode number m becomes

$$-{\omega_m}^2 C_m + 2i\xi_m m\pi\omega_m C_m + m^2\pi^2 C_m = \frac{2(1-\gamma)}{\mathrm{Ma}\, c_0 p_0 \gamma} m\pi \sin(m\pi x_f) Q_m. \tag{28}$$

Q_m denotes the mth exponential term for the heat source model. Let us assume we use one mode (as usually done in a sinusoidal describing function technique – one sinusoidal input to the heat source), then the equation for this mode will be,

$$-\omega^2 C + 2i\xi\pi\omega C + \pi^2 C = \frac{2\left(1-\gamma\right)}{\mathrm{Ma}\, c_0 p_0 \gamma}\pi\sin(\pi x_f)\left(\begin{array}{l} CH_1(\omega)\cos(\pi x_f) \\ +3C^2 D H_3(\omega,\omega,-\omega)\cos^3(\pi x_f) \end{array}\right). \tag{29}$$

We make use of the symmetry of the kernels and the nonlinearity in the heat source can be seen through the third order transfer function. Recall that C and D are complex conjugate numbers and are defined as

$$C = \frac{B}{2} - \frac{A}{2}i, \quad D = \frac{B}{2} + \frac{A}{2}i, \tag{30}$$

with the modal coefficient

$$\eta(t) = A\sin(\omega t) + B\cos(\omega t), \tag{31}$$

where A and B are real numbers. The unknowns of the equation are A, B and ω. Two equations result by equating the imaginary and the real part of the above expression (Eq. 29) to zero. Therefore, there is a need for an extra equation. This problem will be handled by equating for example the real part of the coefficient of the mode to be zero ($B = 0$). That means the phase of the mode is kept at a fixed value.

Let us write the set of equations in detail for a two mode approximation. The equation for the fundamental mode using Eq. 27 and Eq. 28 can be obtained as

$$-\omega^2 C_1 + 2i\xi_1\pi\omega C_1 + \pi^2 C_1 = \frac{2(1-\gamma)\pi\sin(\pi x_f)}{\mathrm{Ma}\, c_0 p_0 \gamma}\left(\begin{array}{l} C_1 H_1(\omega)\cos(\pi x_f) \\ +2C_2 D_1 H_2(2\omega,-\omega)\cos(2\pi x_f)\cos(\pi x_f) \\ +3{C_1}^2 D_1 H_3(\omega,\omega,-\omega)\cos^3(\pi x_f) \\ +6C_1 C_2 D_2 H_3(\omega,2\omega,-2\omega)\cos(\pi x_f)\cos^2(2\pi x_f) \end{array}\right).$$

In the same manner, the equation for the second harmonic can be written as

$$-4\omega^2 C_2 + 4i\xi_2\pi\omega C_2 + 4\pi^2 C_2 = \frac{4(1-\gamma)\pi\sin(2\pi x_f)}{\mathrm{Ma}\, c_0 p_0 \gamma}\begin{pmatrix} C_2 H_1(2\omega)\cos(2\pi x_f) \\ +{C_1}^2 H_2(\omega,\omega)\cos^2(\pi x_f) \\ +6C_1 D_1 C_2 H_3(\omega,-\omega,2\omega)\cos^2(\pi x_f)\cos(2\pi x_f) \\ +3{C_2}^2 D_2 H_3(2\omega,2\omega,-2\omega)\cos^3(2\pi x_f) \end{pmatrix}.$$

The unknowns of the problem are the complex conjugate coefficients $C_1/D_1, C_2/D_2$ and the (real-valued) frequency ω. The number of unknowns are five (two for each of the coefficients and one for the frequency). Four equations are obtained by equating the real and imaginary parts of the above two equations. Again one extra equation for the frequency component can be obtained by equating one of the imaginary parts of the coefficients to zero, i.e. $\Im(C_1) = 0$.

5.2 Interpretation of Modal Coupling

Now, let us take a three mode approximation. In this case, we consider the harmonics $-3\omega, -2\omega, -\omega, \omega, 2\omega, 3\omega$. Then the right hand side of the equation for the fundamental mode will have terms that are coupled through the higher order transfer functions. In this case, the sum of the arguments for the higher order transfer functions will be the fundamental harmonic. Let us write such terms and their meanings in detail:

• $C_2 D_1 H_2(2\omega,-\omega)\cos(2\pi x_f)\cos(\pi x_f)$:
Second mode couples with the fundamental through the second order transfer function

• $C_3 D_2 H_2(3\omega,-2\omega)\cos(3\pi x_f)\cos(2\pi x_f)$:
Third mode couples with the second mode through the second order transfer function

• $C_3 D_1 D_1 H_3(3\omega,-\omega,-\omega)\cos(3\pi x_f)\cos^2(\pi x_f)$:
Third mode couples with the fundamental through the third order transfer function

In general, the contribution of the terms that result in the coupling between the k modes through the nth order transfer function for the fundamental mode equation can be expressed as,

$$S_{d_1}\ldots S_{d_r} H_n \underbrace{(\omega d_1,\ldots,\omega d_r)}_{d_1+\ldots+d_r=1}\cos(\pi d_1 x_f)\ldots\cos(\pi d_r x_f) \quad \text{for } -k \le d_i \le k,\ \ i = 1\ldots r, \tag{32}$$

where S is defined as

$$S_{d_i} = \begin{cases} C_{d_i}, & \text{if} \quad d_i > 0 \\ D_{-d_i}, & \text{if} \quad d_i < 0 \end{cases} \tag{33}$$

The advantage of this type representation of the heat source is that it allows us to find the contribution of the higher harmonics to the fundamental and that it takes various interactions between different harmonics into account.

5.3 Comparison with Time Domain Simulation and Describing Function

Another advantage of the low order model in the frequency domain is that it requires solving a system of nonlinear algebraic equations instead of solving ordinary differential equations with delay terms, which makes a big difference for the computational time. The computational time with the coupled mode frequency domain model has drastically reduced from 10-13 hours (with time domain) to 5-8 minutes. In Fig. 10 above and below are shown the acoustic velocity when the limit cycle is reached obtained from time domain simulation, describing function method and coupled modes frequency domain system model for the heat source located at $0.15L$ and $0.25L$ downstream of the tube inlet, respectively. In the above plot, the discrepancy between the describing function and time domain simulation is large. In the second plot, the second mode instability is suppressed (no contribution from the second mode) and describing function can approximate the amplitude of the limit cycle, but not the shape. In both cases, the coupled modes frequency domain system model captures the amplitude and the shape of the nonlinear oscillation.

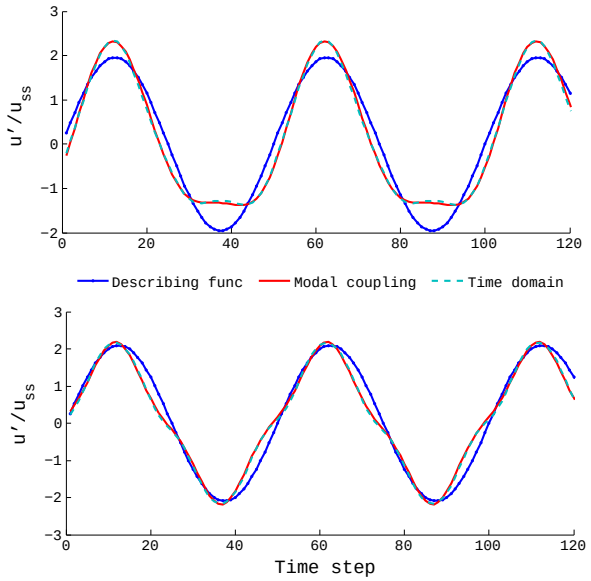

Figure 10: Top - Non-dimensional acoustic velocity at the limit cycle obtained from the time domain simulation (Galerkin), frequency domain coupled modes and describing function method for the initial condition $\eta_1(0) = 0.02$, duct length $L = 5.65$, heat source location $x_f = 0.15$, damping coefficients $c_1 = 0.0135, c_2 = 0.0015$ Bottom - heat source location $x_f = 0.25$

5.4 Rayleigh Index and Energy Balance in the Nonlinear Regime

The energy gained from the heat source will be equal to energy dissipated by the modes when the limit cycle is reached. The energy gained from the local heat source can be directly related to the Rayleigh index which is defined for one cycle of the oscillation as [11, 30],

$$\mathrm{RI} = \frac{1}{T}\int_0^T p' Q' \, dt. \tag{34}$$

Next, we will show how much of the gained energy is distributed among the individual coupling terms. Let us assume a three mode approximation. Substituting the modal representation of the pressure and the nonlinear heat source in the definition of the Rayleigh index results in an expression with 21 terms. First 7 of these terms give the energy gained at the fundamental harmonic, second 7 terms represent the energy gained at the second harmonic and so on.

Energy gained at the second harmonic:

$$\mathrm{RI}_{2\omega} = \Re\left(\frac{2\mathrm{i}\gamma \mathrm{Ma}\,\omega}{\pi} \sin(2\pi \mathrm{x_f}) \left(\begin{array}{l} -D_2 C_2 H_1(2\omega)\cos(2\pi x_f) \\ -2D_2 {C_1}^2 H_2(\omega,\omega)\cos^2(\pi x_f) \\ -2D_2 C_3 D_1 H_2(3\omega,-\omega)\cos(3\pi x_f)\cos(\pi x_f) \\ -6D_2 C_1 C_2 D_1 H_3(\omega,2\omega,-\omega)\cos^2(\pi x_f)\cos(2\pi x_f) \\ -6{D_2}^2 C_1 C_3 H_3(\omega,3\omega,-2\omega)\cos(\pi x_f)\cos(2\pi x_f)\cos(3\pi x_f) \\ -3{D_2}^2 {C_2}^2 H_3(2\omega,2\omega,-2\omega)\cos^3(2\pi x_f) \\ -3D_2 C_2 C_3 D_3 H_3(2\omega,3\omega,-3\omega)\cos(2\pi x_f)\cos^2(3\pi x_f) \end{array} \right) \right). \tag{35}$$

The representation of the heat source in terms of the higher order transfer functions makes it possible to find the effect of the coupling terms. First component of the Rayleigh index gives the energy that is gained by the heat source at the fundamental harmonic. As can be seen for the second element in the second component of the Rayleigh index, energy is driven to the higher harmonics with the nonlinearity. If the system has low pass filter characteristics, the amplitude levels of the higher order harmonics will be small and the coupling terms can be neglected. That is the case where describing function method works. Heat source is generally a low pass filter, but the important is the nonlinearity of the heat source at a specific frequency and amplitude. When only one sinusoid acts as an input to the heat source, it produces higher harmonics and if these components are not suppressed by the system acoustics, the coupling terms appearing in Rayleigh index cannot be neglected anymore. The individual elements of the Rayleigh index for the 21 terms (the terms from 8 to 14 are defined as the individual terms of Eq. (35) for the second component of the Raleigh index) for the third component) are shown in Fig. 11 at the top and bottom for the heat source located at $0.15L$, $0.25L$ downstream of the tube inlet, respectively for a three mode approximation. In the plots, it is also shown the contributions when only one sinusoid acts as the input to the heat source (sinusoidal describing function).

At the top, the second and the fifth terms of the Rayleigh index (energy gained at the fundamental harmonic) have negative contributions (stabilizing effect on the nonlinear oscillations). The eighth and ninth terms of the Rayleigh index (energy gained at second harmonic) have positive contributions (destabilizing effect) and eleventh term has positive contribution. At the bottom, since the second mode instability is suppressed, the fifth, ninth and eleventh terms of the Rayleigh index have no contributions. Energy gained at fundamental, second and third harmonic with the coupling terms via higher order transfer functions included is equal to the energy dissipated by the first, second and the third modes. RI and D represent the gained and damped energies, respectively. As it is shown in table 1, the net energy contributions at the second and third harmonics are positive whereas for the first harmonic it is negative when the heat source is located at $x_f = 0.15L$. For the second configuration ($x_f = 0.25L$), the energy gained at the fundamental harmonic is positive.

For thermo-acoustic systems, it is generally assumed that the energy contribution of the higher order modes can be neglected since the damping factors are large at the higher frequencies. What we have observed is that the coupling terms of the higher order modes can have a stabilizing effect (a negative contribution for the energy gain) or destabilizing effect (a positive contribution to the energy gain). After considering these coupling terms along with the damping can then provide an accurate analysis of the energy balance for the thermo-acoustic systems.

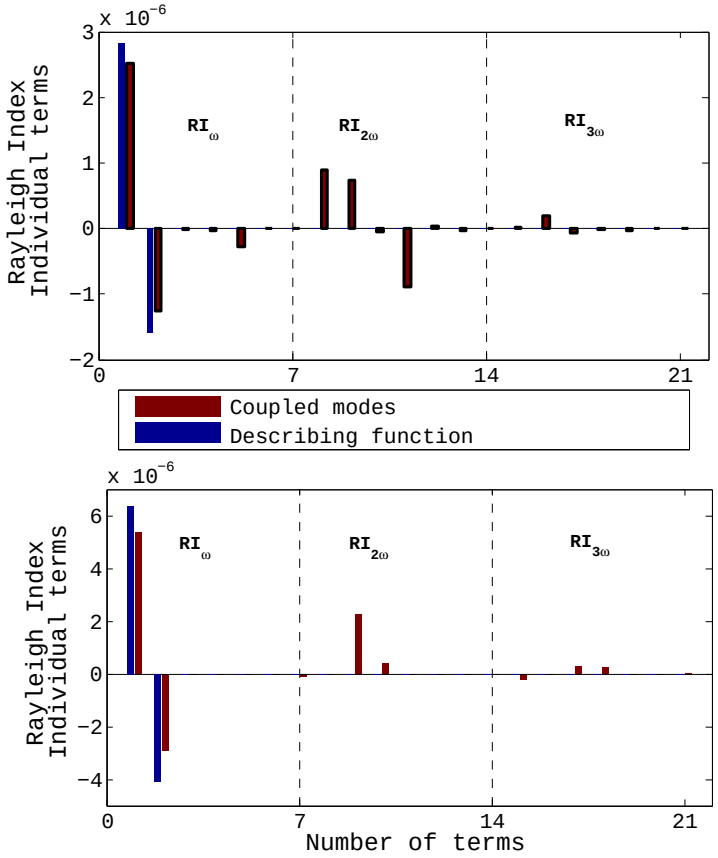

Figure 11: Top: Individual elements of the Rayleigh index for a three mode approximation and describing function, for the duct length $L = 5.65$, heat source location $x_f = 0.15L$, damping coefficients $c_1 = 0.0135, c_2 = 0.0015$. Bottom: heat source location $x_f = 0.25L$

Table 1: Energy gained and damped at different harmonics

	$x_f = 0.15$			$x_f = 0.25$		
	ω	2ω	3ω	ω	2ω	3ω
RI	9.344 E−7	6.959 E−7	0.934 E−7	23.56 E−7	26.7 E−7	2.90 E−7
D	10.05 E−7	6.339 E−7	0.850 E−7	20.76 E−7	29.21 E−7	3.19 E−7
Net Contribution	−0.706 E−7	0.62 E−7	0.084 E−7	2.8 E−7	−2.51 E−7	−0.29 E−7

6 Conclusions and Outlook

In this study, a nonlinear, low order model for thermo-acoustic systems in the frequency domain has been considered. An approach has been developed that can take into account the coupling of the modes due to the nonlinearity. In this method, system variables (acoustic velocity and pressure) are expressed as a superposition of the modes. Nonlinearity in the heat source is expressed in terms of higher order transfer functions. The modes are then coupled through the higher order transfer functions. The equations have been derived using Galerkin method, but an extension of the network models to the nonlinear regime is also possible with this approach. Simulation results have shown one case where the describing function approach fails to predict limit cycle, since the effect of the coupling terms of higher order modes due to the nonlinearity could not be neglected. In this case, coupled modes system model gives the amplitude and the shape of the nonlinear oscillation correctly. Moreover, a reduction in the computational time is achieved from 10-13 hours to 5-8 minutes compared to the Galerkin time domain simulation. An energy balancing of the modes in the limit cycle showed that the coupling terms may give a positive or negative energy contributions. Therefore, an accurate analysis of the energy balance for the thermo-acoustic systems requires to consider the coupling terms along with the damping. The approach has also some drawbacks since the higher order transfer functions are obtained using polynomial type representation of the nonlinearity. The challenges in this approach are described in the following cases:

- when the heat source introduces large delay terms,
- when a large range of frequencies are considered,
- when the approximation of the nonlinearity requires a higher order polynomial degree.

When the network models are extended to the nonlinear regime, then it is possible to add a jump condition in the area/temperature and investigate their effects on the limit cycle amplitudes. A possible coupling of the gas dynamics and the heat source nonlinearity can be investigated, since the system equations have been derived from the Galerkin method, and nonlinear gas dynamics have been derived using Galerkin for second and third order nonlinearities by Culick and co-workers [26,38].

References

[1] K. Balasubramanian and R. I. Sujith. Thermoacoustic instability in a Rijke tube: Non-normality and nonlinearity. *Physics of Fluids*, 20, 2008.

[2] S. Bethke, U.Wever, and W. Krebs. Stability analysis of gas- turbine combustion chamber. In *11th AIAA/CEAS Aeroacoustics Conference*, Monterey, California, 2005.

[3] S.A. Billings. Identification of nonlinear systems - a survey. In *Proceedings of IEEE*, 1980.

[4] S. Boyd and L. O. Chua. Fading memory and the problem of approximating nonlinear operators with Volterra series. *IEEE Transactions on Circuits and Systems*, 32:1150–1161, 1985.

[5] F. E. C. Culick. Non-linear growth and limiting amplitude of acoustic oscillations in combustion chambers. *Combust. Sci. and Tech.*, 3:1–16, 1971.

[6] F. E. C. Culick. Nonlinear behavior of acoustic waves in combustion chambers. parts i and ii. *Acta Astronautica*, 3:715–734,735–757, 1976.

[7] E. Deuker. *Ein Beitrag zur Vorausberechnung des akustischen Stabilitätsverhaltens von Gasturbinen-Brennkammernmittels theoretischer und experimenteller Analyse von Brennkammerschwingungen.* PhD thesis, RWTH Aachen, 1994.

[8] A. P. Dowling. Nonlinear self-excited oscillations of a ducted flame. *J. of Fluid Mechanics*, 346:271–290, 1997.

[9] A.P. Dowling. The calculation of thermoacoustic oscillations. *J of Sound and Vibration*, 180:557–581, 1995.

[10] S. Evesque and W. Polifke. Low-order acoustic modelling for annular combustors: Validation and inclusion of modal coupling. In *Int'l Gas Turbine and Aeroengine Congress & Exposition*, number ASME GT-2002-30064, Amsterdam, NL, 2002.

[11] M. A. Ferreria and J. A. Carvalho. A simple derivation of the rayleigh criterion in integral form. *Journal of Sound and Vibration*, 203(5):889–893, 1997.

[12] Fluent Inc., Lebanon, NH. *FLUENT User's Guide*, 2005.

[13] S. Föller, F. Selimefendigil, and W.Polifke. Linear identification of the unsteady heat transfer of a cylinder in pulsating crossflow. In *Int. Conf. on Jets, Wakes and Separated Flows*, 2008.

[14] A. Gelb and W. E. V. Velde. *Multiple-Input Describing Functions and Nonlinear System Design*. McGraw Hill, 1968.

[15] A. Huber and W. Polifke. Dynamics of practical premix flames, part i: Model structure and identification. *Int. J. of Spray and Combustion Dynamics*, 1:199–229, 2009.

[16] A. Huber and W. Polifke. Dynamics of practical premix flames, part ii: Identification and interpretation of CFD data. *Int. J. of Spray and Combustion Dynamics*, 1:229–250, 2009.

[17] A. Juditsky, H. Hjalmarsson, A. Beneviste, B. Delyon, L. Ljung, J. Sjoberg, and Q. Zhang. Nonlinear black-box models in system identification: mathematical foundations. *Automatica*, 31:1725–1750, 1995.

[18] J. J. Keller. Thermoacoustic oscillations in combustion chambers of gas turbines. *AIAA Journal*, 33:2280–2287, 1995.

[19] M. J. Korenberg, S. B. Bruder, and P. J. McLlroy. Exact orthogonal kernel estimation from finite data records: Extending wiener's identification of nonlinear systems. *Annals of Biomedical Eng.*, 16:201–214, 1998.

[20] K. I. Matveev. *Thermoacoustic instabilities in the Rijke tube: experiments and modeling*. PhD thesis, California Institute of Technology, Pasadena, California, 2003.

[21] K. Narendra and K. Parthasarathy. Identification and control of dynamical systems using neural networks. *IEEE Transactions on Neural Networks*, 1:4–27, 1990.

[22] F. Nicoud, L. Benoit, and C. Sensiau andT. Poinsot. Acoustic modes in combustors with complex impedances and multidimensional active fames. *AIAA J.*, 45:426–441, 2007.

[23] N. Noiray, D. Durox, T.Schuller, and S. Candel. A unified framework for nonlinear combustion instability analysis based on the flame describing function. *J. of Fluid Mechanics*, 615:139–167, 2008.

[24] M. Norgaard, O. Ravn, and N.K. Poulsen. Nnsysid-toolbox for system identification with neural networks. mathematical and computer modelling of dynamical systems. *Mathematical and Computer Modelling of Dynamical Systems*, 8(1):1–20, 2002.

[25] C. Pankiewitz and T. Sattelmayer. Time domain simulation of combustion instabilities in annular combustors. *Transactions of the ASME, Journal of Engineering for Gas Turbines and Power*, (125):677–685, June 2003.

[26] L. G. Paparizos and F. E. C. Culick. The two-mode approximation to nonlinear acoustics in combustion chambers i. exact solution for second order acoustics. *Combustion Science and Technology*, 65 (1):39–65, 1989.

[27] D. T. Pha. *Neural Networks for Identification, Prediction and Control*. Springer, 1995.

[28] W. Polifke. System modelling and stability analysis. In *Basics of Aero-Acoustics and Thermo-Acoustics*, VKI LS 2007-02, Brussels, BE, Dec 3-7 2007. Von Karman Institute.

[29] W. Polifke, A. Poncet, C. O. Paschereit, and K. Döbbeling. Reconstruction of acoustic transfer matrices by instationary computational fluid dynamics. *J. of Sound and Vibration*, 245:483–510, 2001.

[30] A. A. Putnam and W. R. Dennis. Burner oscillations of the gauzetone type. *Journal of the Acoustical Society of American*, 26:716–725, 1954.

[31] M. Schetzen. Measurement of the kernels of a non-linear system of finite order. *International Journal of Control*, 1(3):251–263, 1965.

[32] F. Selimefendigil, S. Föller, and W. Polifke. Nonlinear identification of the unsteady heat transfer of a cylinder in pulsating crossflow. In *Int. Conf. on Jets, Wakes and Separated Flows*, 2008.

[33] Fatih Selimefendigil. *Identification and Analysis of Nonlinear Heat Sources in Thermo-Acoustic Systems*. PhD thesis, TU München, July 2010.

[34] J. Sjöberg, Q. Zhang, L. Ljung, A. Benveniste, B. Delyon, P.Y. Glorennec, H. Hjalmarsson, and A. Juditsky. Nonlinear black-box modeling in system identification: a unified overview. *Automatica*, 31(12):1691–1724, 1995.

[35] L. Tay Wo Chong, R. Kaess, T. Komarek, S. Föller, and W. Polifke. Identification of flame transfer functions using LES of turbulent reacting flows. In *High Performance Computing in Science and Engineering, Garching 2009*, LRZ, Garching, Germany, 2009. Springer.

[36] D. Veynante and T. Poinsot. *Theoretical and Numerical Combustion*. R.T. Edwards, Inc., 2005.

[37] J. Wray and G. G. R. Green. Calculation of the Volterra kernels of non-linear dynamic systems using an artificial neural network. *Biological Cybernetics*, 71:187–195, 1994.

[38] V. Yang, S. I. Kim, and F. E. C. Culick. Triggering of longitudinal pressure oscillations in combustion chambers. i: Nonlinear gasdynamics. *Combustion Science and Technology*, 72 (4):183–214, 1990.

[39] B. T. Zinn and M. E. Lores. Application of the Galerkin method in the solution of non-linear axial combustion instability problems in liquid rockets. *Combust. Sci. and Tech.*, 14:269–278, 1971.